Crystal structures of new silver ion conductors $Ag_7Fe_3(X_2O_7)_4$ (X = P, As)†

Eric Quarez,*[a] Olivier Mentré,[b] Yassine Oumellal[a] and Christian Masquelier[a]

Received (in Montpellier, France) 6th November 2008, Accepted 10th December 2008
First published as an Advance Article on the web 20th January 2009
DOI: 10.1039/b819846b

The crystal structures of new $Ag_7Fe_3(X_2O_7)_4$ (X = P, As) compounds, prepared through ion exchange from their sodium analogs, are reported. They adopt the monoclinic crystal system and exhibit an Ag ordering on cooling evidenced by a lowering of the symmetry from C-centered to primitive Bravais lattices. Crystal structures were determined from single-crystal X-ray diffraction at 100 K and 298 K for each composition. The structure consists of FeO_6 octahedra sharing their corners with P_2O_7 dimers to form a three-dimensional framework $[Fe_3(P_2O_7)_4]^{7-}$ into which the silver ions are located. The differences between the four structures lie on the distribution of the silver ions within this framework, at the origin of a strong anisotropy in conductivity. Temperature displacement factors on Ag sites are generally higher in the arsenate than in the phosphate, in good correlation with conductivity data.

Introduction

Superionic crystalline Ag^+ conductors have been extensively studied these last two decades. One important silver conductor family is the chalcogenide/halide family potentially applied for systems such as electrochemical gas sensors,[1,2] ion-selective electrodes,[3] microbatteries and coulometric devices,[4] and applications in nanostructured memories.[5–7] The compounds generally branch off the superionic compound AgI: Ag_2HgI_4,[8,9] $RbAg_4I_5$,[10] KAg_4I_5,[10] Ag_2CdI_4,[11] Ag_2ZnI_4,[11] Ag_3SnI_5,[11] Ag_4PbI_6,[12] Ag_5Te_2Cl,[13,14] Ag_3SI,[15] $Ag_4Sn_3S_8$,[16] $Ag_{10}Te_4Br_3$.[17,18] Another promising family exhibiting high silver ionic conduction with better thermal stability is represented by the oxide family. A strong interest has been focused on the phosphate compounds with open structure such as Nasicon and related phases $Ag_{1+x}Zr_{2-x}M_x(PO_4)_3$ M = Sc, Fe,[19] $AgTaMP_3O_{12}$[20] (M = Al, Ga, In, Cr, Fe and Y) and compounds with different structures $(Ag_{1-x}Na_x)_2FeMn_2(PO_4)_3$,[21] $Ag_2VP_2O_8$[22] and $AgRu_2(P_2O_7)_2$.[23] The high ionic conductivity of these ceramics can be used in devices such as membranes, fuel cells and gas sensors.[24–26] The other potential applications of this class of compounds include low thermal expansion behavior,[27] as hosts for radioactive waste,[28] catalyst supports,[29] ion exchange[30,31] and insertion/extraction reactions.[32–34]

We reported a decade ago a new family of sodium ion conductors $Na_7M_3(X_2O_7)_4$ (M = Al, Ga, Cr, Fe; X = P, As).[35–37] Among the studied materials, the best conductors were the iron compounds which exhibit conductivity around 10^{-3}–10^{-2} S cm^{-1} at 300 °C. Crystals were grown in a flux of sodium phosphates or arsenates. In the temperature range −20 to 240 °C, depending on M and/or X, they undergo upon heating an α ↔ β reversible phase transition, associated with a loss of long-range ordering of the sodium ions and an increase of the conductivity in the β form. The crystal structures of $Na_7Fe_3(X_2O_7)_4$ (X = P, As) have been determined at room temperature and a model of sodium diffusion paths had already been suggested.

Excellent cationic exchange properties with Ag^+ were also demonstrated.[37] The limit members $x = 7$ of the solid solution $Na_{7-x}Ag_xFe_3(X_2O_7)_4$ (X = P, As) were prepared in molten $AgNO_3$ (in excess) and/or $AgNO_3$ solutions with fixed concentrations that allowed to monitor the value x of Ag^+ ions incorporated in the structure. The two end-members $Ag_7Fe_3(X_2O_7)_4$ (X = P, As) could be isolated as powders and/or single crystals but no detailed structural work on these new compounds had been carried out yet.

The present paper is devoted to the crystal structure determinations of both α and β forms of $Ag_7Fe_3(X_2O_7)_4$ (X = P, As) compounds, *i.e.* measured below and above their respective order–disorder transition temperatures. Several structural characteristics including the splitting of Ag sites, thermal displacement parameters (equivalent and anisotropic), bond valence sums (BVS) and size of oxygen windows separating neighbor Ag sites are discussed and provide qualitative information about the ion mobility.

Experimental

Synthesis

Single crystals of parent compositions $Na_7Fe_3(X_2O_7)_4$ (X = P, As) were first grown by slow cooling (~2 °C h^{-1}) from ~750 to 500 °C and then faster down to room temperature, within a flux of sodium phosphates or arsenates in excess,

[a] *Laboratoire de Réactivité et Chimie des Solides, CNRS UMR 6007, Université de Picardie Jules Verne, 33 rue St. Leu, 80039, Amiens CEDEX, France. E-mail: Eric.Quarez@cnrs-imn.fr*
[b] *UCCS, Equipe Chimie du Solide, CNRS UMR 8181, ENSC Lille – UST Lille, BP 90108, 59652, Villeneuve d'Ascq cedex, France*

† Electronic supplementary information (ESI) available: CIF files and tables of full details of the refinement, atomic parameters, bond valence sums, second and third order displacement parameters for Ag1 in β-$Ag_7Fe_3(P_2O_7)_4$ and β-$Ag_7Fe_3(As_2O_7)_4$ (298 K), distances between neighbor silver sites and size of the oxygen windows for $Ag_7Fe_3(P_2O_7)_4$ and $Ag_7Fe_3(P_2O_7)_4$ at 100 and 298 K. CCDC reference numbers 707710–707713. For crystallographic data in CIF or other electronic format see DOI: 10.1039/b819846b

as indicated in full detail in refs. 35 and 36. Single crystals of $Ag_7Fe_3(X_2O_7)_4$ (X = P, As) were then prepared by ion exchange from $Na_7Fe_3(X_2O_7)_4$ (X = P, As), using an excess of molten $AgNO_3$ for 1 h at ~250 °C. After cooling at room temperature, excess of nitrates were eliminated by extensive rinsing with water. The exchange procedure was repeated twice in order to favor total ion exchange.

X-Ray diffraction

Some of the obtained crystals were selected for structural studies, while others were ground as fine powders so as to check through X-ray powder diffraction that the lattice parameters matched well with those previously reported for powder samples.[37] Powder X-ray diffractograms were collected at room temperature on a Bruker D8 diffractometer using Cu-K$\alpha_{1,2}$ radiation in θ–θ configuration and equipped with a "Super Speed" Vantec Detector discriminated in energy. Data were collected by steps of 0.017° between 2θ = 10 and 70°. Both XRD patterns of β-$Ag_7Fe_3(As_2O_7)_4$ and β-$Ag_7Fe_3(P_2O_7)_4$ are reproduced in Fig. 1. They were easily indexed, using the Fullprof suite,[38] as isostructural with the disordered forms of $Na_7Fe_3(X_2O_7)_4$, *i.e.* in the monoclinic space group $C2/c$ with lattice parameters indicated in Fig. 1.

For single crystals of $Ag_7M_3(X_2O_7)_4$ (X = P, As), X-ray diffraction intensities were collected at low temperature (~100 K) and room temperature (298 K) using Mo-Kα_1 radiation. We used a Bruker SMART CCD 1K diffractometer, equipped with an OXFORD cryostream 700 for data collection at 100 K and a Bruker X8 diffractometer for data collection at 300 K. The global experimental parameters for the four crystal structures determined are gathered in Table 1. The SMART software[39] was used for the data acquisition and SAINT[40] for data extraction and reduction. An absorption correction based on face indexation was then applied using the program Xprep of the SHELXTL package.[41] An additional correction for absorption based on symmetry equivalent reflections was subsequently applied with the program SADABS.[42] The crystal structure solution and refinement processes were carried out with SHELXTL[41] and JANA2000,[43] respectively.

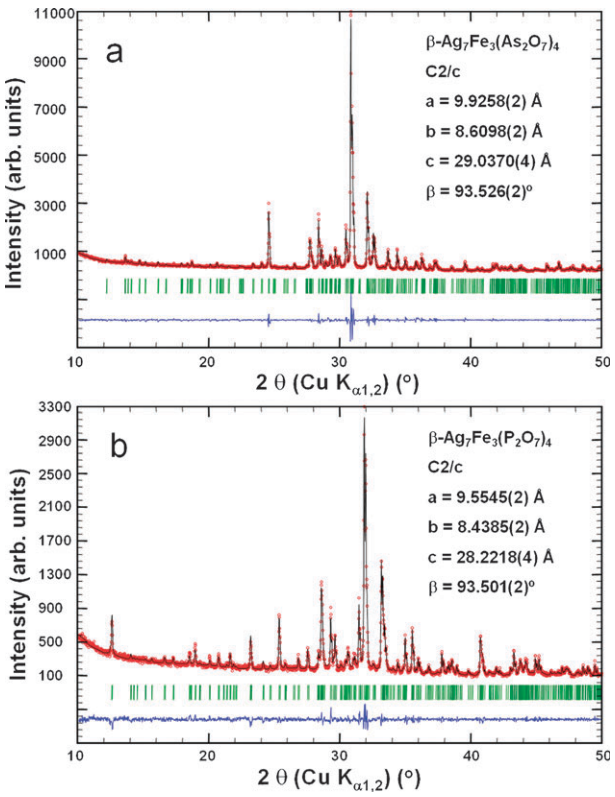

Fig. 1 Observed (markers), calculated (solid line) powder X-Ray diffraction patterns and their difference (bottom line) for β-$Ag_7Fe_3(As_2O_7)_4$ (298 K) and β-$Ag_7Fe_3(P_2O_7)_4$ (298 K).

Conductivity measurements

Experiments of AC conductivity as a function of temperature (300 to 573 K) were performed on ~70% dense pellets of $Ag_7Fe_3(P_2O_7)_4$, under air using a HP 4192 A LF Frequency Analyzer (frequency range of 13 MHz–5 Hz). The pellets were obtained by pressing the powder at 3000 kg cm^{-2} in a uni-axial press, then densified by sustaining an isostatic pressure of 3000 bar for 30 min. Afterwards, the pellet 12 mm in diameter and 1 mm in thickness was sintered at 350 °C for 30 min. Using a Balzer Union SCD40 sputtering apparatus, 100 nm thick Pt layers were deposited on each side of the pellet. A non-linear least-square fitting program included in the ZView software was used to analyze the Cole–Cole plots and to determine the sample resistance defined as the intercept of the Cole–Cole plot with the real axis.

Thermal analysis

DSC measurements were carried out on ~20 mg of powder of $Ag_7Fe_3(P_2O_7)_4$ using a NETZSCH DSC 204 F1 analyzer at temperatures varying from 173 to 773 K with heating and cooling rates of 10 °C min^{-1}. $Ag_7Fe_3(P_2O_7)_4$ undergoes a reversible phase transition at around 280 K (Fig. 2). The presence of hkl reflections with $h + k = 2n + 1$ rules out the C translation mode for the low temperature, α, form of $Ag_7Fe_3(P_2O_7)_4$ that was indexed subsequently in the $P2_1/c$ space group. DSC measurements under the same conditions on $Ag_7Fe_3(As_2O_7)_4$ did not reveal any significant thermal effect although temperature-controlled diffraction clearly revealed the existence of two distinct α and β forms. This suggests that the β → α transition for $Ag_7Fe_3(As_2O_7)_4$ takes place below 173 K.

Results

Crystal structure refinements

Four data sets were recorded from two single crystals of $Ag_7Fe_3(P_2O_7)_4$ and $Ag_7Fe_3(As_2O_7)_4$ at 100 and 298 K. One can notice that the data for the single crystal of $Ag_7Fe_3(P_2O_7)_4$ were affected by a pseudo-merohedral twin due to the value of β close to 90°. The twin corresponds to a rotation about 180° around the reciprocal axis c^*. This was detected using the Cell-now software[44] by indexation of all reflections after the

Table 1 Crystal data, data collection and structure refinement parameters for $Ag_7Fe_3(P_2O_7)_4$ and $Ag_7Fe_3(As_2O_7)_4$ at 100 and 298 K (x = site occupation factor)

	$Ag_7Fe_3(P_2O_7)_4$		$Ag_7Fe_3(As_2O_7)_4$	
T/K	100	298	100	298
M_r/g mol^{-1}	1618.40	1618.40	1969.98	1969.98
Crystal symmetry	Monoclinic	Monoclinic	Monoclinic	Monoclinic
Space group	$P2_1/c$ (no 14)	$C2/c$ (no 15)	$P2_1/c$ (no 14)	$C2/c$ (no 15)
a/Å	9.532(3)	9.5561(5)	9.914(1)	9.9285(3)
b/Å	8.421(2)	8.4417(4)	8.607(1)	8.6101(2)
c/Å	28.021(7)	28.226(1)	28.904(4)	29.0390(8)
β/°	93.225(5)	93.465(2)	93.317(2)	93.523(1)
V/Å^3	2245(1)	2272.8(3)	2462.2(7)	2477.7(2)
Z	4	4	4	4
No. measured reflections	5399	5703	19136	31808
No. independent reflections [$I > 3\sigma(I)$]	3803	5254	4377	7562
R merging factor	5.08	3.44	4.76	4.12
Twin matrix	$\begin{pmatrix} -1 & 0 & 0.33 \\ 0 & -1 & 0 \\ 0 & 0 & 1 \end{pmatrix}$	$\begin{pmatrix} -1 & 0 & 0.3571 \\ 0 & -1 & 0 \\ 0 & 0 & 1 \end{pmatrix}$	—	—
Twin ratio (%)	0.886(1)/0.114(1)	0.893(1)/0.107(1)	—	—
No. refined parameters	402	257	380	276
Eqn. used	—	eqn (2)	eqn (1)	eqn (3)
$R_1(F)$ [$I > 3\sigma(I)$][a] (%)	3.83	4.22	4.09	3.16
$wR_2(F^2)$ [$I > 3\sigma(I)$][b] (%)	4.14	4.69	4.10	3.32

$$x[\mathrm{Ag2b}] = 5 - x[\mathrm{Ag2a}] - x[\mathrm{Ag3a}] - x[\mathrm{Ag3b}] - x[\mathrm{Ag4a}] - x[\mathrm{Ag4b}] \quad (1)$$

$$x[\mathrm{Ag1}] = 1 - x[\mathrm{Ag1'}];\ x[\mathrm{Ag2}] = 2.5 - x[\mathrm{Ag3}] - x[\mathrm{Ag3'}] - x[\mathrm{Ag3''}] - x[\mathrm{Ag4}] - x[\mathrm{Ag4'}] \quad (2)$$

$$x[\mathrm{Ag1}] = 1 - x[\mathrm{Ag1'}];\ x[\mathrm{Ag2}] = 2.5 - x[\mathrm{Ag2'}] - x[\mathrm{Ag3}] - x[\mathrm{Ag3'}] - x[\mathrm{Ag3''}] - x[\mathrm{Ag4}] - x[\mathrm{Ag4'}] - x[\mathrm{Ag4''}] \quad (3)$$

[a] $R_1(F) = \sum||F_o| - |F_c||/\sum|F_o|$. [b] $wR_2(F^2) = [\sum w(F_o^2 - F_c^2)^2/\sum w(F_o^2)]^{1/2}$.

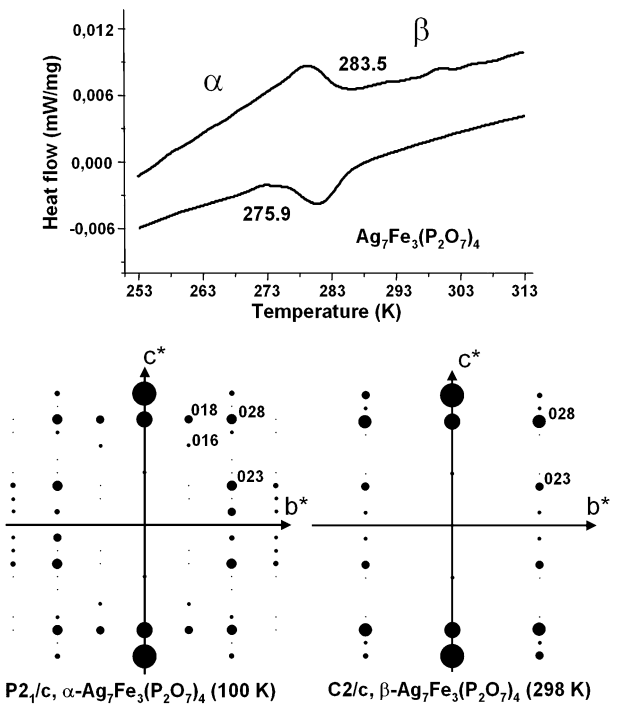

Fig. 2 DSC plots of $Ag_7Fe_3(P_2O_7)_4$ showing a reversible phase transition around 278 K. The $0kl$ layer of the reciprocal space is represented on both sides for α and β forms.

peak hunting stage, using multi-orientation matrices. Then, during the refinement process, only isolated reflections of the domain 1 and overlapping reflections of domains 1 + 2 have been considered, with respect to a maximal angular difference of 0.2°. The twin matrices are given in Table 1 with the details of the ratio for both domains.

α-Forms of $Ag_7Fe_3(P_2O_7)_4$ and $Ag_7Fe_3(As_2O_7)_4$ at 100 K

The crystal system for these two compositions at 100 K is monoclinic as for $Na_7Fe_3(X_2O_7)_4$ (X = P, As).[35,36] The *hkl* list underlines however the presence of reflections with $h + k = 2n + 1$ (Fig. 2), incompatible with the C lattice type observed for $Na_7Fe_3(X_2O_7)_4$. Only a primitive Bravais lattice is hence acceptable and the structures were satisfactorily refined in the $P2_1/c$ space group. The atomic positions of iron, phosphorus and oxygen in $Na_7Fe_3(X_2O_7)_4$ (X = P, As)[35,36] were taken as a starting model (transformed from C to P lattice). The atomic positions of silver were located thanks to the Patterson function calculations as well as subsequent Fourier difference syntheses.

Ag was found to be distributed over seven 4e crystallographic sites in α-$Ag_7Fe_3(P_2O_7)_4$, all fully occupied thus accounting for a completely ordered distribution of silver at 100 K. Globally, the distribution of silver ions resembles that of Na^+ ions within α-$Na_7Fe_3(P_2O_7)_4$[36] except that the Na(3) site located at $z = 0.25$ is here empty. As shown in Fig. 3 and 4,

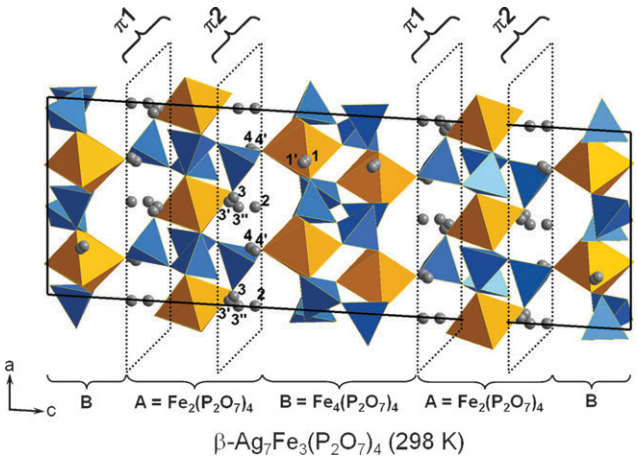

Fig. 3 Projection along [010] of the structure of β-$Ag_7Fe_3(P_2O_7)_4$ (298 K). The silver sites are numbered. The drawing indicates the location of A and B layers, the π planes at $z \sim 0.15$ and ~ 0.35 (equivalent by rotation around a twofold axis in the case of the β forms and 2_1 screw axis in the case of the α forms).

most of Ag^+ ions are located in so-called π planes parallel to (001). One notes from Fig. 4(a) that the Ag(4a) site is fully occupied while its 1/2(***a*** + ***b***) translated position is vacant: this is the main origin of the breaking of the C-Bravais lattice mode.

At the same level of refinement for the arsenate α-$Ag_7Fe_3(As_2O_7)_4$, the reliability factor was not satisfactory. A Fourier difference synthesis revealed very significant electron density at the 4e position (5.18 $e^- Å^{-3}$, $R_1 = 5.40\%$) of the vacancy previously mentioned (labeled as Ag(4b) here). This electron density was introduced in the structural model and its site occupation factor (s.o.f.) was refined. S.o.f. values of all other silver atoms were hence refined as well. It clearly appeared that the Ag(1a) and Ag(1b) sites were fully occupied with an s.o.f. about 0.99: they were subsequently fixed at 1. For the remaining six silver atomic positions, the refined s.o.f. values were below 1, sometimes close to unity. An equation constraining the sum of s.o.f. for these atoms to be equal to 5 (eqn (1) in Table 1, s.o.f. represented as *x*) was introduced in the refinement. In short, contrary to α-$Ag_7Fe_3(P_2O_7)_4$, α-$Ag_7Fe_3(As_2O_7)_4$ does not adopt a fully ordered distribution of Ag^+ ions at 100 K. This will be discussed later in this paper. As a matter of fact, the C-breaking is achieved by comparable effects as previously but with different occupancies related by the 1/2(***a*** + ***b***) translation.

In the last cycles of refinement, anisotropic atomic displacement parameters were considered except for some oxygen atoms and led to very significant improvements of the global reliability factor of the structure. A secondary extinction and unit weighting scheme were introduced leading to reliability factors given in Table 1. Interatomic distances and bond valences sums for Ag^+, Fe^{3+} and X^{5+} (X = P, As) calculated from data from Brown and Altermatt[45] are tabulated in CIF files and Tables of ESI.†

β-Forms of $Ag_7Fe_3(P_2O_7)_4$ and $Ag_7Fe_3(As_2O_7)_4$ at 298 K

The unit cells are C-centered (Fig. 2) and the crystal structures have been successfully refined in the compatible space group *C*2/*c* using the same kind of unit-cell as for β-$Na_7Fe_3(As_2O_7)_4$.[35]

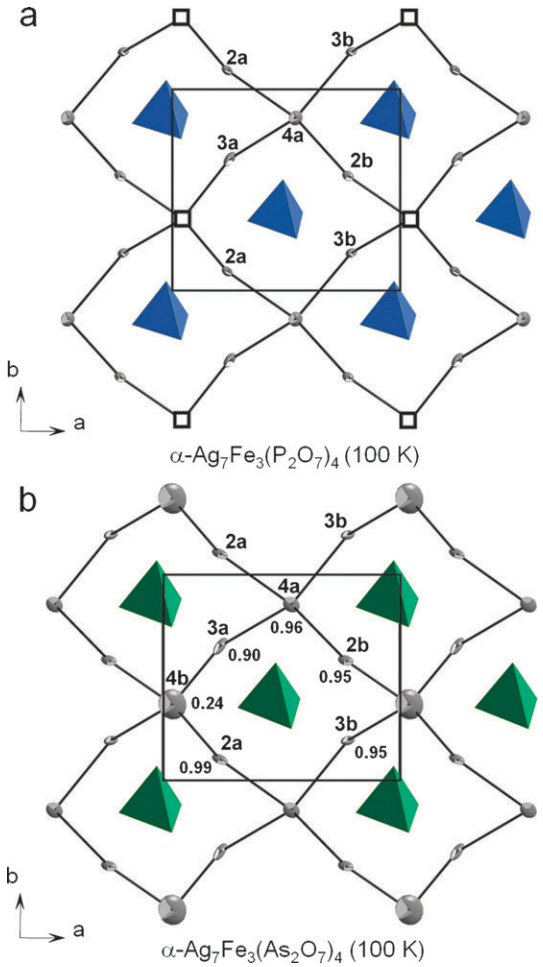

Fig. 4 Silver diffusion paths in the π2 plane of α-$Ag_7Fe_3(P_2O_7)_4$ (a) and α-$Ag_7Fe_3(As_2O_7)_4$ (b) (projection along [001]*). The numbers associated with letters refer to silver sites and numbers alone refer to s.o.f.

Consequently, the initial atomic coordinates of Fe, As or P and O were taken as those of the sodium arsenate phase.[35] Through Fourier difference calculations, several partially occupied sites, all in 8f positions, were found for silver: 8 different sites too close to be simultaneously occupied were found for the phosphate, 10 different sites for the arsenate (Fig. 5). These "electron-density peaks" were introduced in the refinements by refining their s.o.f. Two equations constraining the atoms lying in B "layer" (Ag(1) and Ag1′) to have a s.o.f sum equal to 1 and atoms lying in A layer (Ag2, Ag2′, Ag3, Ag3′, Ag3″, Ag4, Ag4′, Ag4″) to have a s.o.f sum equal to 2.5 were introduced in the refinement (eqn (2) and (3) in Table 1, s.o.f. represented as *x*). Almost all silver sites are split into two or three sites and distances between sites within a doublet or triplet are generally inferior to 1 Å. The distance between Ag1 and Ag1′ for both structures is rather short (~0.2 Å) but the replacement of the doublet by a single site leads to a significant increase of the reliability factors and confirm our choice for split positions. The refinement of the anisotropic atomic displacement parameters for all atoms, a secondary extinction and unit weighting scheme lead to the reliability factors given in Table 1.

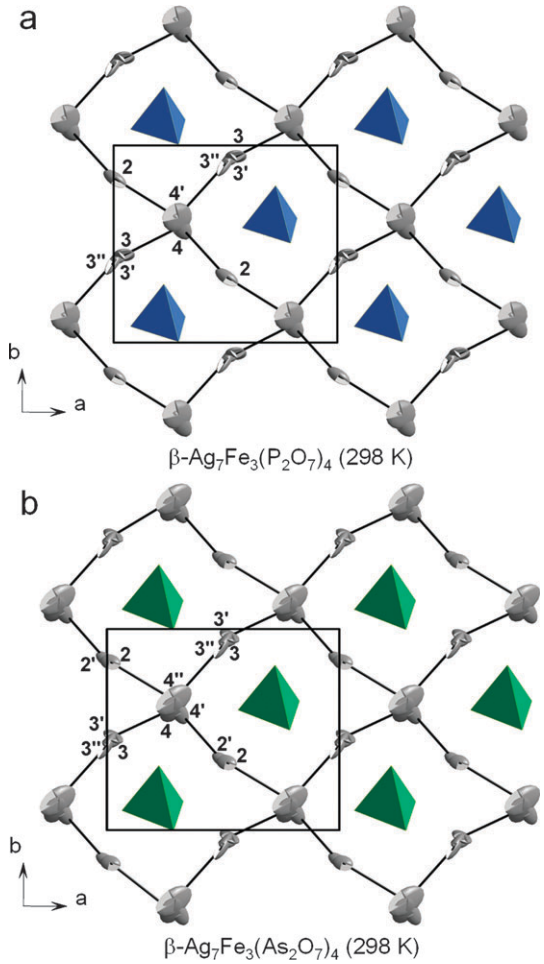

Fig. 5 Silver diffusion paths in the π2 plane of β-$Ag_7Fe_3(P_2O_7)_4$ (a) and β-$Ag_7Fe_3(As_2O_7)_4$ (b) (projection along [001]*). The numbers refer to silver sites.

Discussion

Crystal structures

The basic structure of these series of compounds was first described in ref. 35 and consists of a three dimensional framework $[Fe_3(As_2O_7)_4]^{7-}$ in which the silver ions are inserted. The framework made by FeO_6 octahedra sharing corners with X_2O_7 (X = P, As) dimers can be described by a succession of layers A: $[Fe_2(P_2O_7)_4]^{5-}$ and B: $[Fe_4(P_2O_7)_4]^{2-}$ parallel to (001) (Fig. 3). In the "ordered" α form (100 K) the Ag^+ ions are distributed over seven/eight central positions, mostly fully occupied. In the "disordered" β form (298 K), the Ag^+ ions are distributed over more than eight central positions, mostly partially occupied. Alternatively, the β forms (298 K) may be described as constituted of four "central" positions for Ag, split over satellite positions (Ag(1)–Ag(1′), Ag(3)–Ag(3′)–Ag(3″), ...).

Conductivity properties

The conduction mechanism of silver-based fast ionic conductors lies essentially on the delocalization of the moving species which is favored by (i) low activation energy for "diffusion" from one site to another and (ii) similar site potential energies.[46] An accepted explanation for the usually high mobility of silver in inorganic frameworks is the strong d^{10} cation preference for low coordination.[47] The first discovered silver-based fast ionic conductors were Ag_3SI[48] and $RbAg_4I_5$.[49] More recently, $Ag_{11.88}Cu_{4.12}As_{1.75}Sb_{0.25}S_{11}$[46] and $Ag_{6.69}GeSe_5I_{0.69}$[50] compounds were studied for high silver mobility. Special focus was given to pseudo-potential calculation within the silver diffusion paths.

We investigated the ion transport properties of $Ag_7Fe_3(P_2O_7)_4$ through measurements of electrical conductivity as a function of temperature and compared these new results with those already published in the literature about these structural series. Our data, extrapolated from the analysis of Nyquist plots obtained from complex impedance measurements, are plotted in Fig. 6. They are indicative of an Arrhenius-type behaviour in the temperature range investigated, leading to an activation energy of 0.52 eV (Table 2). Our data fits very well with already measured $M_7Fe_3(X_2O_7)_4$ powders (M = Na, Ag) and trends generally associated with Ag^+ and/or Na^+ inorganic ionic conductors:

- The activation energy is lowered by ~0.1 eV on replacing Na^+ by Ag^+ for a given $M_7Fe_3(X_2O_7)_4$ compound (0.59 to 0.52 for X = P; 0.47 to 0.37 for X = As).
- The total conductivity at 100 or 200 °C of the Ag^+-containing phosphate or arsenate is significantly higher than the corresponding Na^+-containing phosphate or arsenate.
- The total conductivity of arsenates is higher than that of phosphates. This is generally explained by the cell expansion of arsenates ($\Delta V/V$ ~10%) than for phosphates for a given structural family.
- For a given M^+ cation, the α ⇔ β transition occurs at lower temperature for the arsenate than for the phosphate term.
- For a given X = P or As, the α ⇔ β transition occurs at a much lower temperature for the Ag^+-containing compound than for the Na^+-containing compound.

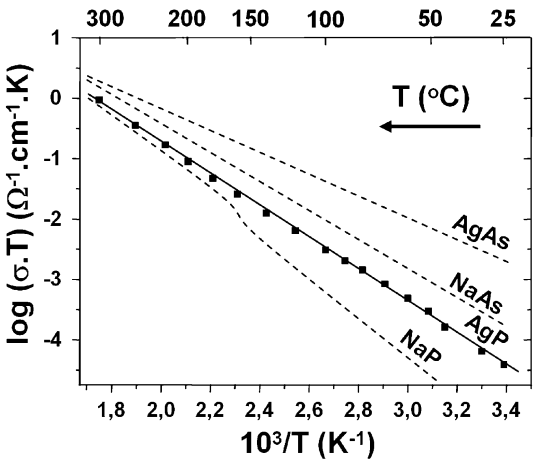

Fig. 6 Temperature dependences in Arrhenius plots of $\log(\sigma T)$ *vs.* $1000/T$ for $Ag_7Fe_3(P_2O_7)_4$ (AgP). Black points are experimental data. The dashed lines represent the temperature dependence for $Ag_7Fe_3(As_2O_7)_4$ (AgAs), $Na_7Fe_3(As_2O_7)_4$ (NaAs) and $Na_7Fe_3(P_2O_7)_4$ (NaP) from ref. 37.

Table 2 Phase transition temperature T_φ, total conductivity σ at 100 and 200 °C and activation energies E_a for $Na_7Fe_3(X_2O_7)_4$ and $Ag_7Fe_3(X_2O_7)_4$ (X = P, As) compounds. Values of σ and E_a of silver conductors reported in the literature are also given

Compound	T_φ/°C	σ(100 °C)/S cm^{-1}	σ(200 °C)/S cm^{-1}	E_a/eV	Ref.
$Ag_7Fe_3(As_2O_7)_4$	<-100	8.8×10^{-5}	9.1×10^{-4}	0.37	37
$Na_7Fe_3(As_2O_7)_4$	−15	2.3×10^{-5}	3.6×10^{-4}	0.47	37
$Ag_7Fe_3(P_2O_7)_4$	5	7.5×10^{-6}	1.9×10^{-4}	0.52	This work
$Na_7Fe_3(P_2O_7)_4$	180	1.4×10^{-6}	1.4×10^{-4}	0.59	37
Ag_2HgI_4		2.0×10^{-4}	—	—	8
$RbAg_4I_5$		3.2×10^{-1}	—	—	10
KAg_4I_5		1.6×10^{-1}	—	—	10
Ag_2CdI_4		1.6×10^{-6}	2.5×10^{-2}	—	11
Ag_2ZnI_4		2.5×10^{-7}	4.0×10^{-4}	—	11
Ag_3SnI_5		2.5×10^{-2}	2.0×10^{-1}	—	11
Ag_4PbI_6		4.0×10^{-4}	1.3×10^{-1}	—	11
Ag_5Te_2Cl		1.6×10^{-1}	4.0×10^{-1}	0.14	13
$Ag_4Sn_3S_8$		3.2×10^{-4}	5.6×10^{-3}	—	16
$Ag_{10}Te_4Br_3$		3.2×10^{-2}	—	—	18
$AgTaFeP_3O_{12}$		8.7×10^{-8}	—	0.70	20
$Ag_2FeMn_2(PO_4)_3$		7.5×10^{-8}	6.1×10^{-6}	0.59	21
$Ag_2VP_2O_8$		1.3×10^{-7}	8.0×10^{-6}	0.58	22
$AgRu_2(P_2O_7)_2$		1.4×10^{-5}	—	0.37	23

It has been already proposed that the mobile Ag^+ cations are located within so-called π parallel planes depicted in Fig. 3–5.[37] Of course, the silver reorganization upon the α → β transition, is an unambiguous signature of the good aptitude of the HT form for conductivity. At this point, it is interesting to note that the transition occurs without drastic change of the lattice parameters, involving a strong rigidity of the $Fe_3(X_2O_7)^{7-}$ framework. This indicates that the cationic paths already exist at low temperature while Ag^+ endures thermally-activated diffusion upon heating. In addition, between the phosphate and arsenate materials, the size of the $Fe_3(X_2O_7)^{7-}$ framework, shows the trend usually observed for other solid electrolytes: the more voluminous paths in the arsenates are in good concordance with the biggest silver site splitting in the arsenate. One notes however that for both phosphate and arsenate compounds, and as for the Na^+-containing counterparts, the Ag(1) site located within the more dense "B-layer" (not within the π diffusion planes) is less affected by the order–disorder transition and hence should be less involved in the overall ionic conduction.

Split-site models *versus* anharmonicity

The non-harmonic approach has been successfully used over the past twenty years in solving numerous structures, including both non-mobile species[51–53] and fast ion conducting compounds.[13,14,54–56] The validity of an anharmonic model against a distribution of sites more or less pictures a dynamic disordering against a static one. From a crystallographic point of view, the appropriate choice is ruled on by several parameters including R values, n. of parameters that increase with the n^{th} order of the anharmonic treatment, the correlation between them, residual e^- density, ... Then the refinement of both room-temperature forms have been tested by modelling the residual electronic density around the central Ag^+ cations using the Gram–Charlier development of the atomic displacement parameter. The comparison between both models is in favour of a split distribution of silver centres at this temperature considering comparable convergences with a lower number of refined parameters:

$Ag_7Fe_3(P_2O_7)_4$	Split	R = 4.22%, n_{param} = 257
	Anharmonic (Ag1: 3rd order, Ag2: 2nd order, Ag3/4: 4th order)	R = 4.10%, n_{param} = 277
$Ag_7Fe_3(As_2O_7)_4$	Split	R = 3.16%, n_{param} = 276
	Anharmonic (Ag1/2: 3rd order, Ag3/4: 4th order	R = 3.51%, n_{param} = 286

It is noteworthy that for both compounds, the distributed model leads to high correlation (>0.9) between Ag1 and Ag1′ coordinates, due to their close position. However, it was checked on F_{obs} Fourier maps, that the shape of the anharmonic thermal parameters corresponds well to the sum of Ag1 and Ag1′ ellipsoids with no significant deviations.

A high-temperature study of the $Ag_7Fe_3(As_2O_7)_4$ compound treated with anharmonic approach is currently in progress. To establish further relationships between the structure and the properties of this family of ionic conductors, we undertook a detailed examination of several parameters such as the thermal parameters (U_{eq}, U_{aniso}) and the bond valence sums applied to Ag^+. The size of the oxygen windows which separate neighbor Ag sites were also compared with each other.

Diffusion paths

The analysis of thermal ellipsoids (U_{eq} and U_{aniso}) correlated to the bond valence sum (BVS) calculation (Table 3) gives a preliminary picture of the cationic mobility for each silver site from which several interesting trends may be highlighted, especially for the "disordered" structures measured at 298 K.

Table 3 Equivalent thermal parameters U_{eq} and bond valence sums of silver atoms for β-$Ag_7Fe_3(P_2O_7)_4$ (298 K) and β-$Ag_7Fe_3(As_2O_7)_4$ (298 K)

	β-$Ag_7Fe_3(P_2O_7)_4$		β-$Ag_7Fe_3(As_2O_7)_4$	
	U_{eq}/Å^2	BVS	U_{eq}/Å^2	BVS
Ag1	0.0196	1.115	0.0179	1.065
Ag1′	0.027	1.138	0.0216	1.082
Ag2	0.0334	0.838	0.0259	0.802
Ag2′			0.024	0.878
Ag3	0.06	0.864	0.0477	0.774
Ag3′	0.039	0.865	0.22	0.924
Ag3″	0.046	0.839	0.0497	0.741
Ag4	0.049	0.937	0.051	0.861
Ag4′	0.066	0.821	0.0374	0.965
Ag4″			0.084	0.75

(i) The Ag1 type sites systematically appear "overbonded" (BVS > 1) assorted with the smallest thermal ellipsoid while all other split silver type atoms appear consistently "underbonded" (BVS < 1). It is noteworthy that the size of the "oxygen windows" around Ag(1) on the way to other silver sites averages to a value of 2.00 to 2.05 Å, much smaller than the commonly accepted value of $r(Ag^+) + r(O^{2-})$ = 2.45 Å (Fig. 7(a)).

(ii) Ag2, Ag3 and Ag4 type sites show ellipsoids lying in the in π-planes with vibrational elongations along the paths shown on the Fig. 5. This "vibration" would represent the most probable silver diffusion paths circumventing the XO_4 tetrahedra obstacles and following two possible directions $\sim\vec{a} + \vec{b}$ and $\sim\vec{a} - \vec{b}$. Ag4 type sites with rather spherical thermal ellipsoids would play the role of "crossroads". It is noticeable that the thermal ellipsoids of silver atoms are much more developed in the case of the room-temperature refinements than the low-temperature ones validating the thermally-activated mobility. Interestingly, around Ag4, the size of the "oxygen windows" averages to 2.19–2.23 Å, much bigger that for the Ag1 sites (Fig. 7(b)).

(iii) For both compounds, one split atom of the Ag3 type forms a strongly anisotropic "cigar"-like ellipsoid oriented towards the parallel π-plane (along the [001] direction), suggesting a favorable π1 to π2 bridge (Fig. 7(c)). Hence, while ionic transport in this family of compounds is strongly anisotropic (2-D, within π planes parallel to (001)),[35–37] π planes are connected perpendicular to (001) through the Ag(3′)–Ag(3′) sequence.

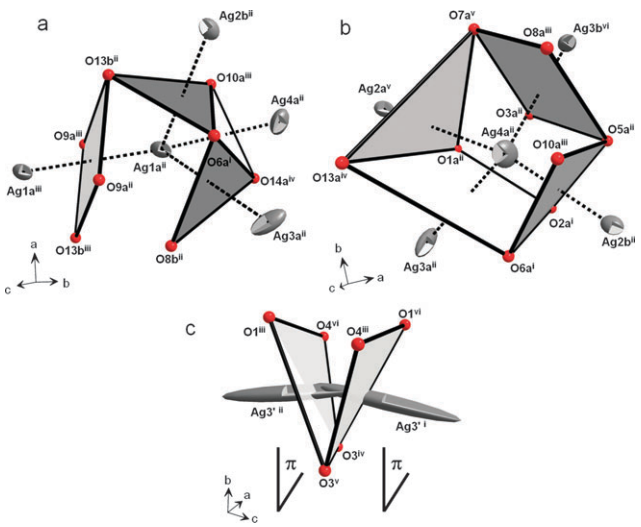

Fig. 7 Drawing of the oxygen windows separating silver atoms from Ag1 type atoms (a), Ag4 type atoms (b) represented for α-$Ag_7Fe_3(P_2O_7)_4$ (100 K) and between Ag3 type atoms (c) represented for β-$Ag_7Fe_3(As_2O_7)_4$ (298 K). Equivalent-position for α-$Ag_7Fe_3(P_2O_7)_4$ (100 K): (i) x, y, z; (ii) $1 - x$, $0.5 + y$, $0.5 - z$; (iii) x, $0.5 - y$, $0.5 + z$; (iv) $1 - x$, $1.5 + y$, $0.5 - z$; (v) x, $1 + y$, z; (vi) $1 + x$, $1 + y$, z. Equivalent-position for β-$Ag_7Fe_3(As_2O_7)_4$ (298 K): (i) x, y, z; (ii) $1 - x$, y, $0.5 - z$; (iii) x, $1 + y$, z; (iv) $0.5 + x$, $0.5 + y$, z; (v) $0.5 - x$, $0.5 + y$, $0.5 - z$; (vi) $1 - x$, $1 + y$, $0.5 - z$.

Conclusion

In the last decade, only a few compounds in the system Ag_2O–Fe_2O_3–X_2O_5 (X = P, As) have been reported in the literature. So far, two compounds not pointed out in ref. 37 were prepared and characterized: $AgFeP_2O_7$[57] and $AgFeAs_2O_7$.[58]

We reported in the present paper the crystal structure of $Ag_7Fe_3(P_2O_7)_4$ and $Ag_7Fe_3(As_2O_7)_4$ at 100 and 298 K. Close relationships between structure and cation transport properties were established showing silver diffusion paths are favored in π planes and between close π planes in A layers but are difficult in B layers. This study, besides establishing the crystal structures of four new iron phosphates/arsenates, provides useful information on ionic transport in 3-D frameworks by indicating here:

(1) the Ag sites within the structures that are more likely to conduct,

(2) the pathways followed by the mobile Ag^+,

(3) the influence of the temperature,

(4) the material with the best level of conductivity.

The resulting conclusions are in very good agreement with the conductivity measurements. Further work will focus on the investigation of diffusion paths from one site to another in terms of pseudo-potential calculations, taking into account the high-temperature modification of the structure.

Acknowledgements

The authors are grateful to Dr M. Morcrette for his help in conductivity measurements and K. Djellab for DSC measurements. The "Fonds Européen de Développement Régional (FEDER)", "CNRS", "Région Nord Pas-de-Calais" and "Ministère de l'Education Nationale de l'Enseignement Supérieur et de la Recherche" are acknowledged for funding of single-crystal X-ray diffractometers at the UCCS, Villeneuve d'Ascq, France.

References

1 K. Nagashima and N. Nakano, *Zairyo Gijutsu*, 1997, **15**, 146.
2 S. S. Sunu, V. Jayaraman, E. Prabhu, K. I. Gnanasekar and T. Gnanasekaran, *Ionics*, 2004, **10**, 244.
3 K. Cammann and H. Galster, in *Das Arbeiten mit Ionenselektiven Elektroden*, 3rd edn, Springer, Berlin, 1996, p. 71.
4 T. Takahashi, in *Handbook of Solid State Batteries & Capacitors*, ed. P. S. S. Prasad and M. Z. A. Munshi, World Scientific, Hackensack, NJ, 1995, pp. 79–109.

5 M. N. Kozicki, M. Mitkova, M. Park, M. Balakrishnan and C. Gopalan, *Superlattices Microstruct.*, 2003, **34**, 459.
6 C.-U. Pinnow and T. Happ, *Ger. Pat.*, DE 102004014965, 2005.
7 C.-U. Pinnow, T. Mikolajick, T. Happ and R. Symanczyk, *Ger. Pat.*, DE 10323414, 2004.
8 S. Hull and D. A. Keen, *J. Phys.: Condens. Matter*, 2000, **12**, 3751.
9 S. Hull and D. A. Keen, *J. Phys.: Condens. Matter*, 2001, **13**, 5597.
10 S. Hull, D. A. Keen, D. S. Sivia and P. Berastegui, *J. Solid State Chem.*, 2002, **165**(2), 363.
11 S. Hull, D. A. Keen and P. Berastegui, *J. Phys.: Condens. Matter*, 2002, **14**, 13579.
12 S. Hull, D. A. Keen and P. Berastegui, *Solid State Ionics*, 2002, **147**, 97.
13 T. Nilges, S. Nilges, A. Pfitzner, T. Doert and P. Böttcher, *Chem. Mater.*, 2004, **16**, 806.
14 T. Nilges, C. Dreher and A. Hezinger, *Solid State Sci.*, 2005, **7**, 79.
15 S. Matsunaga and P. A. Madden, *J. Phys.: Condens. Matter*, 2004, **16**, 181.
16 S. Hull, P. Berastegui and A. Grippa, *J. Phys.: Condens. Matter*, 2005, **17**, 1067.
17 S. Lange and T. Nilges, *Chem. Mater.*, 2006, **18**, 2538.
18 S. Lange, M. Bawohl, D. Wilmer, H.-W. Meyer, H.-D. Wiemhöfer and T. Nilges, *Chem. Mater.*, 2007, **19**, 1401–1410.
19 J. Angenault, J. C. Couturier and M. Quarton, *Mater. Res. Bull.*, 1989, **24**(7), 789.
20 K. Koteswara Rao, G. Rambabu, M. Raghavender, G. Prasad, G. S. Kumar and M. Vithal, *Solid State Ionics*, 2005, **176**(37), 2701.
21 A. Daidouh, C. Durioa, C. Pico, M. L. Veigaa, N. Chouaibi and A. Ouassini, *Solid State Sci.*, 2002, **4**, 541.
22 A. Daidouh, M. L. Veiga and C. Pico, *J. Solid State Chem.*, 1997, **130**, 28.
23 H. Fukuoka, H. Matsunaga and S. Yamanaka, *Mater. Res. Bull.*, 2003, **38**, 991.
24 M. Meunier, R. Izquierdo, L. Hasnaoui, E. Quenneville, D. Ivanov, F. Girard, F. Morin, A. Yelon and M. Paleologou, *Appl. Surf. Sci.*, 1998, **127**, 466.
25 S. Yao, Y. Shimizu, N. Miura and N. Yamazoe, *Chem. Lett.*, 1990, 2033.
26 R. Collongues, A. Khan and D. Michel, *Annu. Rev. Mater. Sci.*, 1979, **9**, 123.
27 J. Alamo and R. Roy, *J. Mater. Sci.*, 1986, **21**, 444.
28 R. Roy, E. R. Vance and J. Alamo, *Mater. Res. Bull.*, 1982, **17**, 585.
29 A. Serghini, A. Kacimi, M. Ziyad and R. Brochu, *J. Chem. Phys.*, 1988, **85**, 499.
30 N. Hirose and J. Kuwano, *J. Mater. Chem.*, 1994, **4**, 9.
31 A. Nadiri and C. Delmas, *C. R. Acad. Sci. Paris*, 1987, **304**, 9.
32 C. Delmas, F. Cherkaoui, A. Nadiri and P. Hagenmuller, *Mater. Res. Bull.*, 1987, **22**, 631.
33 C. Delmas, A. Nadiri and J. L. Soubeyroux, *Solid State Ionics*, 1988, **28**, 419.
34 J. Gopalakrishnan and K. Kasturi Rangan, *Chem. Mater.*, 1992, **4**, 745.
35 C. Masquelier, F. D'Yvoire and N. Rodier, *Acta Crystallogr., Sect. C*, 1990, **46**, 1584.
36 C. Masquelier, F. D'Yvoire and N. Rodier, *J. Solid State Chem.*, 1991, **95**, 156.
37 C. Masquelier, F. D'Yvoire, E. Bretey, P. Berthet and C. Peytour-Chansac, *Solid State Ionics*, 1994, **67**, 183.
38 J. Rodriguez-Carjaval, Fullprof suite 2000, LLB (CEA-CNRS), France.
39 SMART, Siemens Analytical X-ray Systems, Inc., Madison, WI 53719.
40 SAINT + Version 6.02: Area-Detector Integration Software, Siemens Industrial Automation, Inc., Madison, WI, 1998.
41 G. M. Sheldrick, SHELXTL NT, version 5.1, Bruker Analytical X-ray Systems, 1998.
42 SADABS: Area-Detector Absorption Correction, Siemens Industrial Automation Inc., Madison, WI, 1996.
43 V. Petricek, M. Dusek and L. Palatinus, *The crystallographic computing system 2000*, Institute of Physics, Praha, Czech Republic, 2000.
44 G. M. Sheldrick, CELL NOW program for unit cell determination, Göttingen University, 2000.
45 I. D. Brown and D. Altermatt, *Acta Crystallogr., Sect. B*, 1985, **41**, 244.
46 L. Bindi, M. Evain, A. Pradel, S. Albert, M. Ribes and S. Menchetti, *Phys. Chem. Miner.*, 2006, **33**, 677.
47 E. Gaudin, F. Boucher and M. Evain, *J. Solid State Chem.*, 2001, **160**, 212.
48 B. Reuter and K. Hardel, *Z. Anorg. Allg. Chem.*, 1965, **340**, 158.
49 B. B. Owens and G. R. Argue, *Science*, 1967, **157**, 308.
50 R. Belin, L. Aldon, A. Zerouale, C. Belin and M. Ribes, *Solid State Sci.*, 2001, **3**, 251.
51 A. Vanderlee, F. Boucher, M. Evain and R. Brec, *Z. Kristallogr.*, 1993, **203**, 247.
52 F. Boucher, M. Evain and R. Brec, *J. Alloys Compd.*, 1994, **215**, 63.
53 E. Gaudin, L. Fischer, F. Boucher, M. Evain and V. Petricek, *Acta Crystallogr., Sect. B*, 1997, **53**, 67.
54 W. F. Kuhs, *Acta Crystallogr., Sect. A*, 1992, **48**, 80.
55 F. Boucher, M. Evain and R. Brec, *J. Solid State Chem.*, 1992, **100**, 341; F. Boucher, M. Evain and R. Brec, *J. Solid State Chem.*, 1993, **107**, 332; M. Evain, E. Gaudin, F. Boucher, V. Petricek and F. Taulelle, *Acta Crystallogr., Sect. B*, 1998, **54**, 376; M. Evain, L. Bindi and S. Menchetti, *Acta Crystallogr., Sect. B*, 2006, **62**, 768; M. Evain, L. Bindi and S. Menchetti, *Acta Crystallogr., Sect. B*, 2006, **62**, 447; L. Bindi, M. Evain and S. Menchetti, *Acta Crystallogr., Sect. B*, 2006, **62**, 212; L. Bindi, M. Evain and S. Menchetti, *Can. Mineral.*, 2007, **45**, 321; L. Bindi and M. Evain, *Am. Mineral.*, 2007, **92**, 886.
56 T. Nilges, S. Reiser, J. H. Hong, E. Gaudin and A. Pfitzner, *Phys. Chem. Chem. Phys.*, 2002, **4**, 5888; T. Nilges and S. Lange, *Z. Anorg. Allg. Chem.*, 2005, **631**, 3002; S. Lange and T. Nilges, *Chem. Mater.*, 2006, **18**, 2538; S. Lange, M. Bawohl, D. Wilmer, H.-W. Meyer, H.-D. Wiemhöfer and T. Nilges, *Chem. Mater.*, 2007, **19**, 1401–1410.
57 J. Belkouch, L. Monceaux, F. Oudet, E. Bordes and P. Courtine, *Mater. Res. Bull.*, 1990, **25**(9), 1099.
58 N. Ouerfelli, M. F. Zid, T. Jouini and A. M. Touati, *J. Soc. Chem. Tunis.*, 2004, **6**(1), 85.